Electrospinning fabricated novel pyrene-based aggregation-induced emission luminogens (AIEgen) composite fiber as phase change materials for thermal energy storage

Jintao Huang[1,#,*], Yiwei Liu[1,#], Jiahui Lin[1], Jingtao Su[1], Carl Redshaw[2], Xing Feng[1,*], Yonggang Min[1,*]

[1] School of Materials and Energy, Guangdong University of Technology, Guangzhou 510006, China.

[2] Chemistry, School of Natural Sciences, University of Hull, Cottingham Road, Hull, Yorkshire, HU6 7RX, UK.

[*]Corresponding authors (E-mail: jintao.huang@gdut.edu.cn (J. Huang); hyxhn@sina.com (X. Feng); ygmin@gdut.edu.cn (Y. Min))

[#]These authors contributed equally to this work.

Abstract

Advanced multifunctional composite materials have been a significant force in the advancement of efficient solar-thermal energy conversion and storage, which is critical to address current energy shortage problems. In this study, new pyrene-based AIEgens composite fiber films, composed of **Py-CH**/polyvinyl pyrrolidone (PVP)/polyethylene glycol (PEG) (APP) have been produced by electrospinning technology with PEG as the phase-change material. The combination of AIE and the twist intermolecular charge transfer (TICT) characteristics of **Py-CH** together with the water absorption performance of PVP afforded a temperature-dependent fluorescence change. On increasing the temperature from 30 to 160 ºC, the APP composites exhibit a blue-shifted emission with a color changed from green-yellow to cyan, from cyan to blue, and finally to purple. Moreover, the pyrene-based AIEgens composite fiber films with a PEG content of about 60% exhibited latent heat in the range of 79~89 $J \cdot g^{-1}$ and were extremely stable for up to 100 heating-cooling cycles. On the other hand, the entanglement of the macromolecular chains and distinctive porous structure between PVP and PEG play a significant role in preventing the leakage and transfer issues that can be associated with PEG, which further promotes the application of these APP composites in solar energy storage, high-temperature warning, and anti-counterfeiting applications. Thus, these composite materials containing the pyrene-based AIEgen and phase change materials have opened up new avenues for the possible application of such materials in thermal energy storage.

Keywords: Electrospinning; Aggregation-induced emission; Phase change materials; Thermal energy storage; Applications

1 Introduction

Advanced composites materials, assembled by two or more materials, [1, 2] are now one of the hot research topics in modern technology, [3, 4] and have wide applications in fields such as energy conversion and storage. [5, 6] Thermal energy storage (TES), involving enhancing the reliability of thermal energy from renewable sources, is one of the key technologies to support the large-scale development of renewable energy. [7-9] As a crucial component of the TES system, phase change materials (PCMs) have been considered as one of the most promising candidates for thermal energy storage via the storage or release of a great amount of latent heat. [10, 11] Nevertheless, several issues, such as leakage of PCMs in their liquid state, low thermal conductivity, and poor thermal stability, have hindered their commercial viability. [12] In order to solve the above issues, advanced shape-stable phase change composites have been prepared via combining PCMs with supporting materials [13] and various functional additives (e.g., thermal management materials, [14] fluorescent materials [15] and so on). In addition, processing methods have also been developed in order to shape composites materials into fibers, [16] foams, [17] aerogels, [18] etc., for advanced applications. Polyethylene glycol (PEG), is low cost, has high latent heat enthalpy, a wide transition temperature range, possesses thermal and chemical stability, and has a suitable phase change temperature, and so is widely considered to be the most promising solid-liquid organic PCMs for energy storage. [19-22] The addition of different additives is an effective strategy to remove the obstacles that limit the practical application of PCMs and can also be employed to achieve the functionalization of PCM composites. To address the issue of low thermal conductivity, many efforts have focused on the addition of high thermal conductive fillers, such as expanded graphite, silver nanowires, carbon nanotubes, etc. [23-26] Interestingly, the use of fluorescent materials, which may allow for the PCM composites to possess yet more intriguing properties, have attracted little attention.

In contrast, fluorescent dyes with aggregation-induced emission (AIE) characteristics, defined by Tang and coworkers in 2001, [27] emit weak fluorescence in solution and enhance the fluorescence intensity in the aggregate states. Thus, the discovery of AIE can be an important approach for solving the ACQ effect and should widen the possibilities for traditional applications. [28] Recently, explorations concerning the combination of AIE emission luminous (AIEgen) and PCM composites for potential application have been investigated. For example, Liu *et al*. first investigated the combination of PCM composites and AIE materials in a phase change material system. The fluorescent thermochromic PCM materials exhibited visual solar-thermal energy conversion and storage. [15] Also, Yang reported the preparation of cellulose nanofiber-encapsulated PEG-based PCM composites containing AIEgen for the monitoring of the leak process. [29] However, the preparation of PCM@AIE composites and the realization of their potential application still remains a challenge, due to the limitations associated with the processing methods and the temperature-dependence of the AIEgens.

Pyrene, [30, 31] an important member of polycyclic aromatic hydrocarbons (PAHs), possesses bright blue fluorescence with a high quantum yield, and has been widely applied to various applications, e.g, OLEDs, [32] chemosensors, [33] anti-counterfeiting [34] etc. Also, pyrene is sensitive to the microenvironment, and this leads to visible emission changes. On the other hand, the π-conjugated planar structure of pyrene prefers to form π-π stacking, resulting in a red-shifted emission with a quenched quantum yield, and this is termed aggregation-caused quenching, which has limited its high-technological application. Thus, by utilizing the excellent fluorescence of pyrene with the AIE characteristic, a pyrene-based AIE fluorophore could be a great candidate for sensing changes in the microenvironment, such as temperature, and external stimulation, etc.

Benefiting from the advantages of versatility, flexibility and ease of processing, electrospinning is able to fabricate continuous composite fibers from a huge range of mixed materials, which make it stand out from other processing methods for PCM composites. [35] For instance, polyvinyl alcohol/phase change material fibers with reliable thermoregulating performance were prepared by an emulsion electrospinning technique. [36] The fiber integrity was maintained even if the PCM melted after heat treatment, which solved the leakage problem. Sodium lignosulfonate/polyvinyl alcohol/polyethylene glycol phase-change nanofiber films, exhibiting high latent heat of fusion and favorable shape stability, were also constructed using electrospinning technology. [37] In the above two studies, polyvinyl alcohol, a non-toxic water-borne polymer, was chosen as the matrix material. What's more, polyvinyl pyrrolidone was used as the fiber matrix given its better solubility in water and organic solvents, as well as good physiological compatibility. For example, novel polyethylene glycol/graphene oxide composite phase-change fibers were developed by using PVP as the fiber matrix via electrospinning to enhance the thermal properties of shape-stabilized PCM fibers. [24] It is evident that the introduction of electrospinning technology has promoted the progress of PCM composites.

Herein, we have constructed novel pyrene-based AIEgens composite fiber films (APP) using electrospinning and have evaluated the temperature-dependent fluorescence behavior and potential application in thermal energy storage. The composite fiber is composed of PEG (PCM material), PVP (matrix material), pyrene-based AIEgen **Py-CH** (fluorescent additive) and a small amount of boron nitride (BN) (for improving thermal conductivity). It was found that the APP composites not only possess thermal energy storage properties and photo-thermal conversion performance, but also exhibit temperature-dependent fluorescence behavior. This all results from the combination of the AIE and TICT characteristics of **Py-CH** and the water absorption performance of PVP. Due to the above excellent properties, three promising applications, including solar-to-thermal conversion and storage, high-temperature warning, and anti-counterfeiting, were explored.

2 Experimental section

The preparation process of the AIEgen/PVP/PEG composite (APP) fiber films is shown in Figure 1. Firstly, 12 wt% PVP and 18 wt% PEG were added into 10 mL DMF with stirring at 60 °C until the PVP and PEG were completely dissolved. A homogeneous solution with the PEG and PVP molecular chains winding each other was obtained. Secondly, a certain amount of BN and **Py-CH** were added into the mixture and stirred for 12 h at 60 °C. During this process, the PEG was grafted with BN and **Py-CH** by the insertion of BN and **Py-CH** between the PEG and PVP molecules. Thirdly, the solution was placed into a plastic syringe with a 22 stainless-steel needle and was transformed into fiber films by electrospinning technology. During the electrospinning, the rotation speed of the receiving roller was 50 r/min, the collector distance was 20 cm, the voltage difference was 21 kV, and the flow rate of the solution was kept at 0.008 mm/s. Finally, in order to remove DMF, the obtained APP composite fiber films were placed in a vacuum oven at 90 ºC for 24 h. In this experimental procedure, we tried to find the influence of the content of AIE on this novel composite material so that three fiber films with different contents of **Py-CH**, including 0.046 wt%, 0.075 wt%, and 0.104 wt%, were prepared and were assigned as APP046, APP075, and APP104 respectively. More detailed information on the experimental procedure and characterization can be found in the Supporting Information.

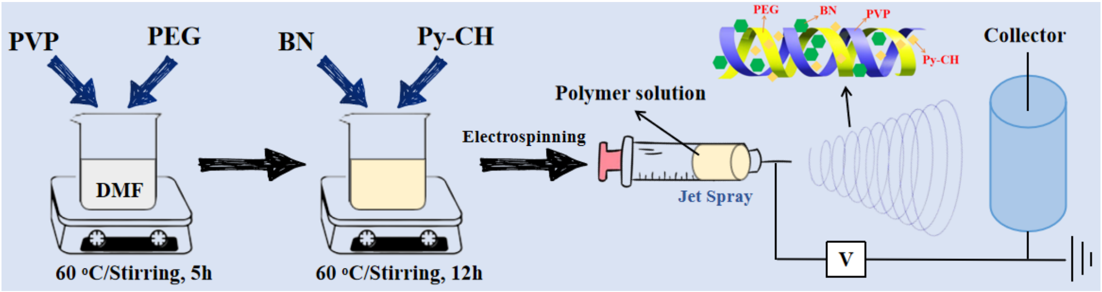

Figure 1. Electrospinning preparation process of APP fiber films.

3 Results and discussion

3.1 Synthesis of the pyrene-based emitter Py-CH

As shown in Figure 2 (a), the target compound **Py-CH** was synthesized following the synthetic route shown. The intermediate 2-*tert*-butyl-7-hydroxypyrene (**Py-OH**) was prepared from 2-*tert*-butylpyrene via two steps (borylation and oxidation reaction) in high yield. [38] Then, using the Lewis acid catalyst $ZnCl_2$, a domino one-pot reaction of **Py-OH** with 4-ethynyl-*N*,*N*-dimethylaniline afforded the chromenes **Py-CH** in considerable yield. [39] The molecular structure of **Py-CH** was characterized by $^{1}H/^{13}C$ NMR spectroscopy and high-resolution mass spectrometry (HRMS), as shown in Figures S1-S3. The electron distributions of compound **Py-CH** were investigated by density functional theory (DFT) calculations at the B3LYP/6-31G (d,p) level. As shown in Figure 2 (b), the HOMO and LUMO are separated and almost dispersed over the chromene unit and pyrene ring, respectively. It seems that the chromene and pyrene act as electron-donating (D) and electron withdrawing groups (A), respectively, which would result in a pull-push molecular structure with fantastic optical behavior.

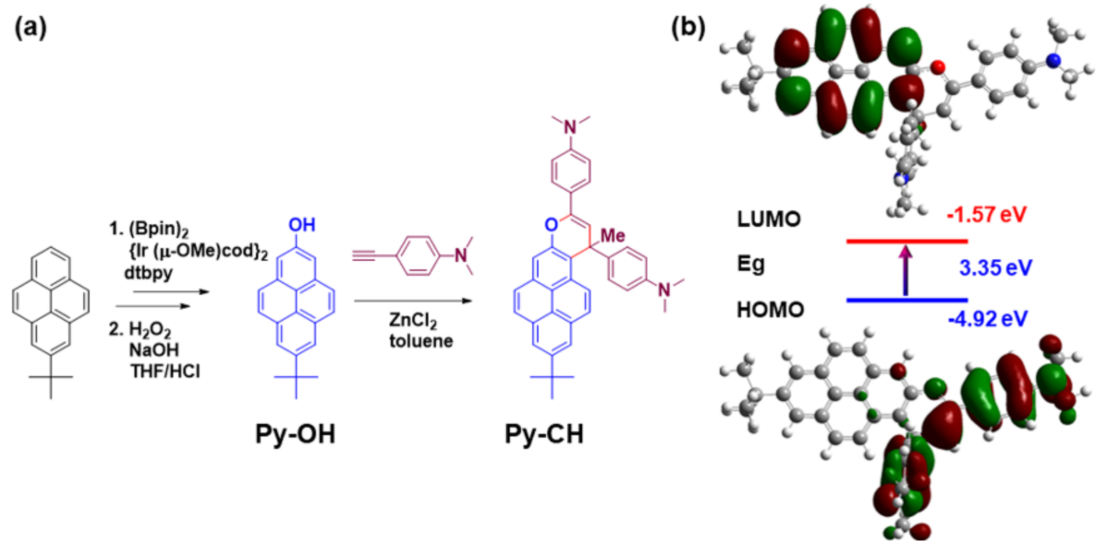

Figure 2. (a) Synthetic route of **Py-CH**; (b) Electron distributions of compound **Py-CH**.

3.2 Photophysical properties of Py-CH

The UV-vis absorption and PL spectra were measured in dilute THF solution and in the solid state at room temperature (Figure 3 (a)). Compared to the unsubstituted pyrene, the compound **Py-CH** exhibits a well-defined absorption band with red-shifted absorption bands at 259 nm and 374 nm with a shoulder absorption peak at 355nm and 409 nm, which can be ascribed to the expanding π-conjugation skeleton. [40] Upon excitation, the compound emits green emission with a maximum emission peak at 520 nm in THF solution, and the quantum yield is as low as 0.06. While the emission intensity was enhanced with a blue-shift to 493 nm ($\Phi_f = 0.08$) in the solid state compared to in THF solution, which can be ascribed to the formation of H-aggregation in the solid state. [41] The solvatochromic effect was further measured in six different polarity solvents and is illustrated in Figure 3 (b). Except in DMSO solvent, as the solvent polarity increases, the **Py-CH** displays a large bathochromic-shifted emission (*ca*. 152 nm) from non-polar cyclohexane (Cy) (429 nm) to polar solvent ACN (581 nm), indicating that the compound is a typical electron donating-accepting type organic molecule, which exhibits an intramolecular charge transfer (ICT) process, where the pyrene acts an electron-withdrawing group, and the chromene unit is an electron-donating group. This result is consistent with the DFT calculations.

On the other hand, due to the enhanced solubility in DMSO, the compound **Py-CH** exhibits a dual emission peak at 420 nm with a broaden emission peak at 595 nm. The short-wavelength emission peak may be assigned to the pyrene skeleton, and the long-wavelength emission peak originates from the charge-transfer (CT) emission, as shown in Table S1. As the viscosity increases from 0% to 99%, the molecular rotation was fixed and the molecule became more rigid, leading to the emission being red-shifted from 420 to 495 nm (Figure 3 (c)). Furthermore, the concentration-dependent PL spectra in THF were recorded in order to understand the molecular aggregation behavior. As shown in Figure S4, the compound exhibits a single emission peak at 431 nm, whilst as the concentration increased, dual emission with maximum emission peaks at 413 and 513 nm were observed at 10^{-6} M. When the concentration reached 10^{-5} M, the compound displays a single emission peak with a red-shifted emission at 520 nm, which can be assigned to excimer emission. This indicated that the compound **Py-CH** prefers to form a dimer when the concentration is up to 10^{-5} M.

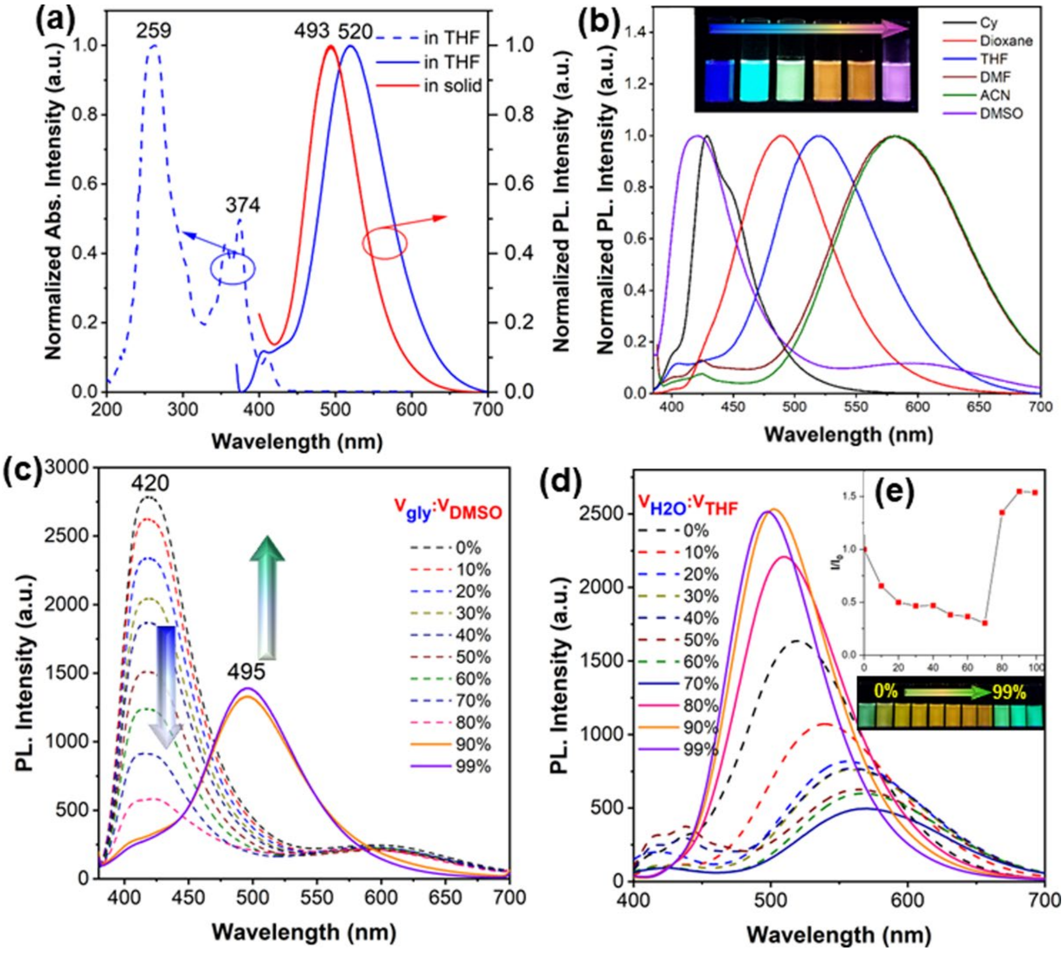

Figure 3. (a) UV-vis and emission spectra of compound **Py-CH** in THF (~10^{-5} M) and in the solid state; (b) PL spectra of **Py-CH** measured in different polar solvents, insert: the fluorescent photograph of **Py-CH** in different polar solvents under UV light (λ_{ex} = 365 nm) and (c) measured in DMSO/glycerol solutions ($f_{\text{DMSO/glycerol}}$) with different viscosities and (d) PL spectra of **Py-CH** in THF/water mixtures with different water fractions (f_w); (e) Plot

of relative PL intensity (I/I_0) *versus* the composition of a THF/water mixture. Insert: the fluorescent photograph of **Py-CH** with different f_w under UV light (λ_{ex} = 365 nm).

Previously, Konishi *et al.* found that the highly twisted *N*,*N*-dialkylamine decorated anthracene, naphthalene and pyrene can play a significant role to stabilize the S_1/S_0 minimum energy conical intersection (MECI), and can induce fantastic aggregation-induced emission characteristics. [42, 43] Inspired by the molecular structure of **Py-CH**, the AIE characteristics of **Py-CH** were investigated in a THF/H_2O mixture with different water fractions (f_w). As shown in Figure 3 (d,e), the compound emits weak green emission in pure solvent, and the emission intensity was quenched with a large bathochromic-shift emission band from 520 to 569 nm when the f_w increased from 0 to 70%. This may be ascribed to the ICT effect, and as the f_w increases to 99%, the emission intensity rapidly enhanced with a blue-shifted emission to 497 nm. Clearly, compound **Py-CH** displays a typical aggregation-induced enhanced emission (AIEE) feature. The compound shows a hyperchromic-shift emission in the aggregation state (f_w = 99%), which can be explained as the formation of hydrophobic aggregates excluding the polarity solvent molecules, resulting in the AIE effect overwhelming the ICT effect. The calculated radiative decay rate (k_r) of **Py-CH** is slightly decreased from 1.23×10^7 s^{-1} to 0.62×10^7 s^{-1} ($\approx$0.5-fold), while the nonradiative decay rate (k_{nr}) is decreased by more than 2.6-fold, as shown in Table S2. Thus, the **Py-CH** is an AIEE-active material.

3.3 Fluorescence properties of the pyrene-based AIEgen/PVP/PEG (APP) composite fiber films

APP composite fiber films not only possess enhanced thermal properties, but also attain excellent fluorescence properties due to the addition of the AIEgen. In order to prove the presence of the **Py-CH** in the composites, three samples were placed under UV light at room temperature (about 20 °C). Clearly, all three of the APP composites emitted green-yellow fluorescence in dark conditions under UV irradiation, as shown in Figure 4. This implies that **Py-CH** was successfully distributed on the composites and endowed the composites with fluorescence. What’s more, it is interesting to note that the fluorescent color of the composites changed when the temperature was varied. On increasing the temperature, the fluorescent color gradually changes to a shorter wavelength color, from green-yellow to cyan, from cyan to blue, and finally to purple. Based on the fluorescence response to temperature, we propose that the initial hypothesis is that the combination of PEG and AIE can achieve the conversion of thermal energy and fluorescence energy. Specifically, PEG, as a phase change material, converts the thermal energy into molecular motion energy, driving the movement of the AIE molecules, thus achieving the fluorescence changes.

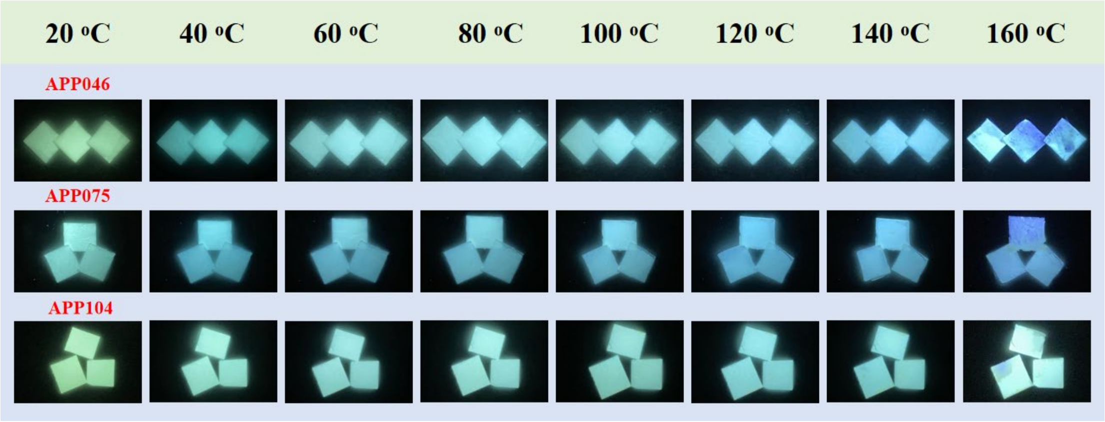

Figure 4. The fluorescence photographs of APP046, APP075, and APP104 under different temperature.

To further explore the properties of the APP composite fiber films affected by the additional AIEgen (**Py-CH**), the fluorescence properties of the APPs were investigated by fluorescence spectra under different temperatures, as shown in Figure 5 (a,b), Figures S5 (a) and S6 (a). On increasing the temperature, a significant decrease in the fluorescence intensity of **Py-CH** was observed, while the fluorescent emission peak is invariable. The fluorescent emission peak of **Py-CH** almost disappeared when the temperature reached 130 °C. This indicates that the fluorescence responses of the APP composites do not result from the fluorescence responses of **Py-CH** to thermal changes. In contrast to pure **Py-CH**, the fluorescent emission peak of the three APP composites were blue-shifted when the temperature increased, implying a change of fluorescent color. It is clearly seen that there is an obvious blue-shift trend for the fluorescent colors of the APP composites from Figure 5 (c), Figures S5 (b) and S6 (b). What’s more, the higher the content of **Py-CH**, the smaller the fluorescence color change span, which is further confirmed in Figure 8. More importantly, the fluorescence intensities of the APP046 and APP075 composites increased instead of decreasing like **Py-CH**. Moreover, the weakening trend of fluorescent intensity of the APP104 composite was greatly reduced. Based on the above analysis, we find that there is an appropriate addition amount range for **Py-CH** (0.046~ 0.075 wt.%) to enable the composite to display a better variable temperature fluorescence response. To sum up, the composites not only achieve a blue-shift of fluorescence color with increasing temperature, but also inhibit the disadvantage of thermal failure (decrease of fluorescence intensity) of pure **Py-CH**, enabling it to be applied at a certain temperature. At present, according to above analysis, we still speculate that PEG plays an important role in the variable temperature fluorescence properties of the composites.

However, the TGA of PEG, PVP, and the three composites overturns the previous hypothesis. In the TG curve of PVP under a nitrogen atmosphere (Figure 5 (d)) till 150 °C, there was just a mass loss of ~ 10%, which can be assigned as the loss of physically adsorbed water. [44] The molecule chains of the PVP contain polar lactam groups, which have the ability to create dipole-dipole interactions with water molecules. [45] In other words, the PVP possesses great water-absorption performance, and the water-absorption isotherm of the PVP increases almost linearly until RH = 0.6. After 0.6 RH, there is a slight upward curvature of the water-absorption isotherm. [46] After incorporating PVP, there also exists a mass loss of ~ 10% on the TG curve of the three APP composites, which resulted from the loss of adsorbed water and a very small amount of solvent that was used during the electrospinning. After that, in the TG curve of all samples, only one larger step could be seen between 400 ºC and 600 ºC, indicating the great thermal stability of the composites. Most notably, the temperature range for the water-loss of the composites was remarkably consistent with that of its variable temperature fluorescence. The TG analysis lead us to reject the previous hypothesis and open a new door of exploration. Variation of the amount of water adsorbed by PVP in the composite may lead to the response of fluorescence to thermal changes.

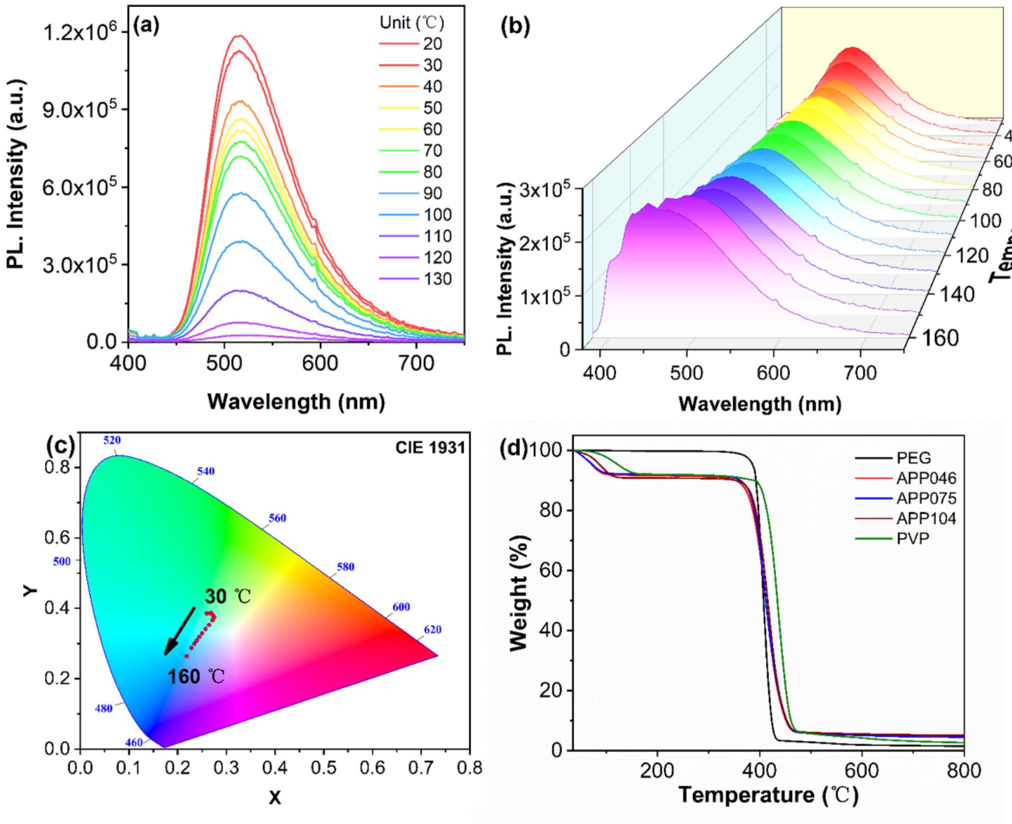

Figure 5. Fluorescence spectra of (a) **Py-CH** and (b) APP075 under different temperatures; the CIE chromatogram of (c) APP075 under different temperatures; (d) TG analysis of PEG, PVP, and three APPs.

The above evidence revealed the mechanism of the variable temperature fluorescence of composites. On the one hand, water with high polarity has an influence on the emission behavior of **Py-CH**. On the other hand, there was a certain linear relationship between temperature and water fraction for the composites in the TG curve. As shown in Figure 6, at the outset, the water in the air is absorbed into the composite fiber film due to the water absorption performance of PVP, resulting in an enhanced polar environment in the film. In the polar environment, the composites exhibit yellow-green fluorescence with longer wavelength. Then, with the increase of temperature, the evaporation of the adsorbed water gradually enhanced. Finally, the decrease of wavelength of fluorescence (blue-shift) is observed as a result of the TICT mechanism and the increase of fluorescent intensity due to the typical AIE nature. [47] A 240-second fluorescent recyclable experiment of APP104 also echoed the above mechanism. After heating at 80 °C for 30 seconds, the fluorescent color of the APP104 composite fiber film was blue-shifted due to the evaporation of adsorbed water. The fluorescent color of the composite returns to its original color after cooling at room temperature for 210 seconds as a result of the strong water-absorption performance of PVP. Variable temperature fluorescence and the fluorescent recyclable of the APP composite fiber films suggests they are promising for use in high-temperature warning and anti-counterfeiting applications.

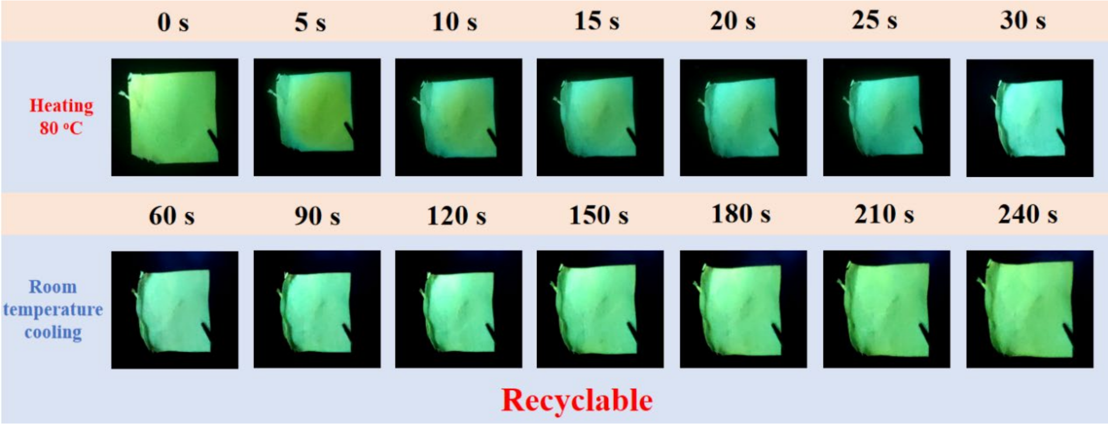

Figure 6. The digital photograph of recyclable experiment of APP104.

3.4 Morphology of the pyrene-based AIEgen/PVP/PEG (APP) composite fiber films

The surface morphologies of the APPs were examined by SEM, as shown in Figure 7. Also, the diameter distribution histograms of the APPs were counted. It was observed that the fibers interweave with each other into a three-dimensional network structure. There is redundant PEG adhesion on the surface of the fibers and filled in the pores, which indicates that the homogeneous solution has been successfully transformed into a fiber film via electrospinning and the PEG has been mixed into composites. The PEG is not only mixed with PVP to form fibers [24], but also its excess part is tightly confined by the pores of the fiber network, which not only achieves a high PEG package rate, but also effectively prevents the PEG leakage during the phase-change procedures. The average diameters for APP046, APP075, and APP104 are 3.482 ± 1.006, 3.652 ± 1.162, and 3.471 ± 1.579 μm, respectively. The amount of AIEgen has little effect on the diameter of the fibers, and the diameter of the three samples generally vary over the range 2~5 μm. Actually, the content of PEG is the most important factor affecting the diameter of the fiber. The addition of PEG would increase the concentration of the solution and make the elongation of the Taylor cone formed under the action of the electric field force become somewhat more difficult and slower, which enlarges the diameter of fibers. [37] Because the content of PEG in the three samples is almost the same, their average fiber diameters are similar under the same spinning parameters.

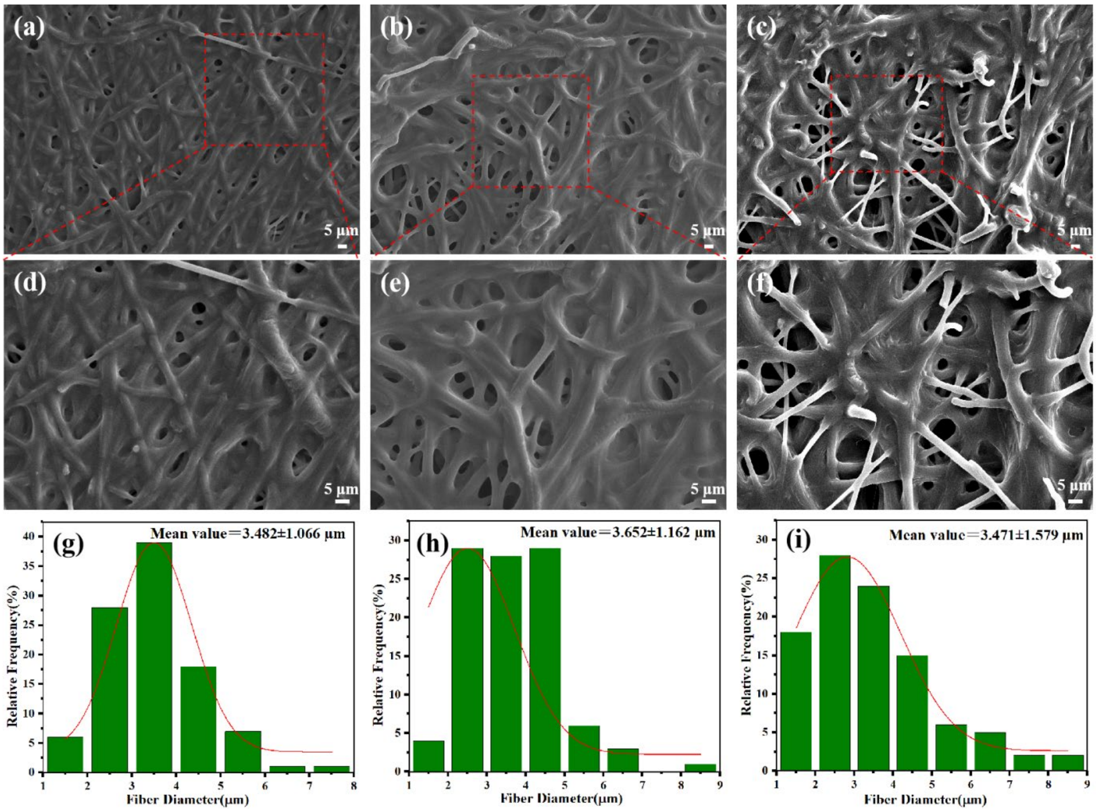

Figure 7. SEM images and their enlarged SEM views of AIEgen/PVP/PEG composites (APPs) with different AIEgen contents: (a,d) 0.046 wt%, (b,e) 0.075 wt%, (c.f) 0.104 wt%. The diameter distribution histograms of (g) APP046, (h) APP075, (i) APP104.

3.5 Structural characterization of the pyrene-based AIEgen/PVP/PEG (APP) composite fiber films

FT-IR spectroscopy was used to investigate the chemical structure of the novel APP composite fiber films. Figure 8 (a) shows the FT-IR spectra of PEG, PVP, **Py-CH**, and the APP composites with different **Py-CH** content. Similar to PEG, the three APPs represented the characteristic peaks of 2900, resulting from the stretching vibrations of C-H groups. The band of PEG and APPs at 3434 cm^{-1} was related to the stretching vibration of O-H. The peak for the APPs at 1099 cm^{-1} is assigned to the C-O-C symmetrical stretching vibrations of PEG. Moreover, the PAAs also possesses very similar characteristic peaks with PEG in the range of 1530~740 cm^{-1}. Examples include 1467 and 955 cm^{-1}, which can be attributed to the bending vibration and rocking vibration of C−H from PEG, respectively. The absorption peak of PVP at 1654 cm^{-1} assigned to the C=O stretching vibration also appears for the APPs. The FT-IR spectra of **Py-CH** and the APPs, circled by the red sign, are analogous. In a word, the FT-IR spectra indicates that all characteristic peaks of PEG, PVP, and **Py-CH** appear in the APPs without any new characteristic peaks, thus the PAA composite fiber films were successfully fabricated through electrospinning and there is no chemical reaction taking place.

The crystal structure has a significant influence on the properties of a material. The XRD patterns of PEG, PVP, BN, **Py-CH** and the APP075 composite fiber film are displayed in Figure 8 (b). Two sharp diffraction peaks for pure PEG are observed at 2θ of about 19.1° and 23.2°, indicating that PEG has good crystallization. The BN displays a notable sharp peak at 26.7°. There exists a diffraction peak at 11.2° in the XRD pattern of PVP. From the diffraction patterns of the APP075 composite, it can be seen that PEG still shows two diffraction peaks at 19.1° and 23.2°, which means that the crystal plane distance was nearly the same and the crystal structure of PEG is well maintained in the composite and its crystal structure was not affected by BN and **Py-CH**. However, compared with pure PEG, the peak intensity decreases in the presence of other components like PVP. To be specific, hydrogen bonds between PEG and PVP are formed, restricting the crystallization of PEG and reducing the peak intensity. Besides, the XRD pattern of APP075 includes the weak diffraction peak at 11.2°, resulting from the PVP existing in the APP075. Furthermore, typical diffraction peaks appeared at 26.7° in pure BN and the APP075 composite, which indicated that the BN was well mixed into the APP075. **Py-CH** exhibits peaks at 23.2°, indicating a highly crystalline state, whereas the PAA composite does not, due to the minimal **Py-CH** content in the composite. In conclusion, there was no new diffraction peak in the PAA075 composite, indicating that there was no chemical reaction between all the components, and only physical blending occurred. This result is consistent with that of the FT-IR spectroscopy.

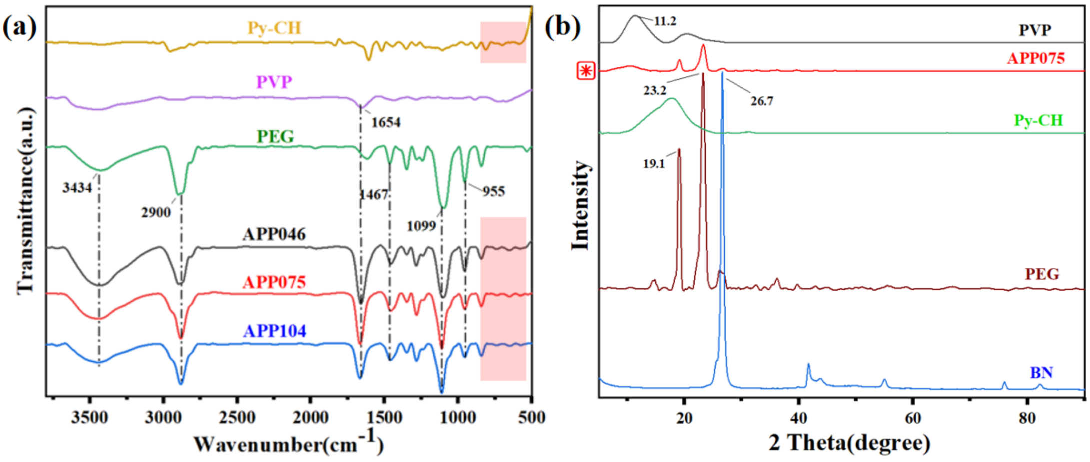

Figure 8. (a) FT-IR spectra of **Py-CH**, PVP, PEG and three APP composites with different **Py-CH** contents: APP046, APP075, APP104; (b) XRD patterns of PVP, **Py-CH**, PEG, BN, and the APP075 composite fiber film.

3.6 Thermal energy storage and thermal reliability of the pyrene-based AIEgen/PVP/PEG (APP) composite fiber films

As is well-known, thermal properties plays an important role in practical applications of thermo-regulated composite fiber films. The thermal storage capacity of pure PEG, APP046, APP075, and APP104 were investigated by DSC experiments. The obtained DSC results are presented in Figure 9 (a-c), and the corresponding phase-change temperature and latent heat during melting/crystallization process obtained from DSC analyses are listed in Table 1. Typical endothermic and exothermic peaks can be observed for all specimens (pure PEG and three APP composites) in Figure 9 (a), which represents the phase change process of the PEG. Such a phenomenon is attributed to the coexistence of amorphous and crystalline phases during the crystal transformation. [24] Besides, the melting and freezing temperature (phase change temperature) of pure PEG and three composites reveal only a neglectable difference, as shown in Figure 9 (b) and Table 1. However, there exists some disparities between the theoretical value and the real value of the phase transformation enthalpy of composites.

The theoretical value of the phase transformation enthalpy of the APP composites can be calculated by equation (1). [37]

$$\Delta H_{APPs} = \Delta H_{PEG} \times \omega \tag{1}$$

where ω (≈0.6) refers to the mass fraction of PEG in the composites, ΔH_{APPs} and ΔH_{PEG} represent the phase transition enthalpy of the APP composites and pure PEG, respectively. Compared with the theoretical value of the phase transformation enthalpy (ΔH_{APPs}), it is found that the real value of the phase transformation enthalpy of all three APP composites (ΔH_{APPs}') is slightly lower, which can be seen visually in Figure 9 (c). This may result from the water absorption of PVP. [48] With the increase mass fraction of water absorbed by PVP [49], the ω value would decrease accordingly, meaning that the position for PEG is occupied by water so that the value of the phase transformation enthalpy of the composites decrease. Fortunately, due to the limited amount of water absorption when the composites are under an atmospheric environment, the enthalpy value of the composites will be stable over the range 79~89 J/g, and the enthalpy value will not be very low. Generally, the DSC thermograms of all APP composites are similar to those of pure PEG, although the real value of the phase transformation enthalpy has a slight decrease during the heating or cooling process, implying that the interior PEG of the composites could conduct the regular phase change behavior and the APP composite fiber films can be used as a thermal energy storage material.

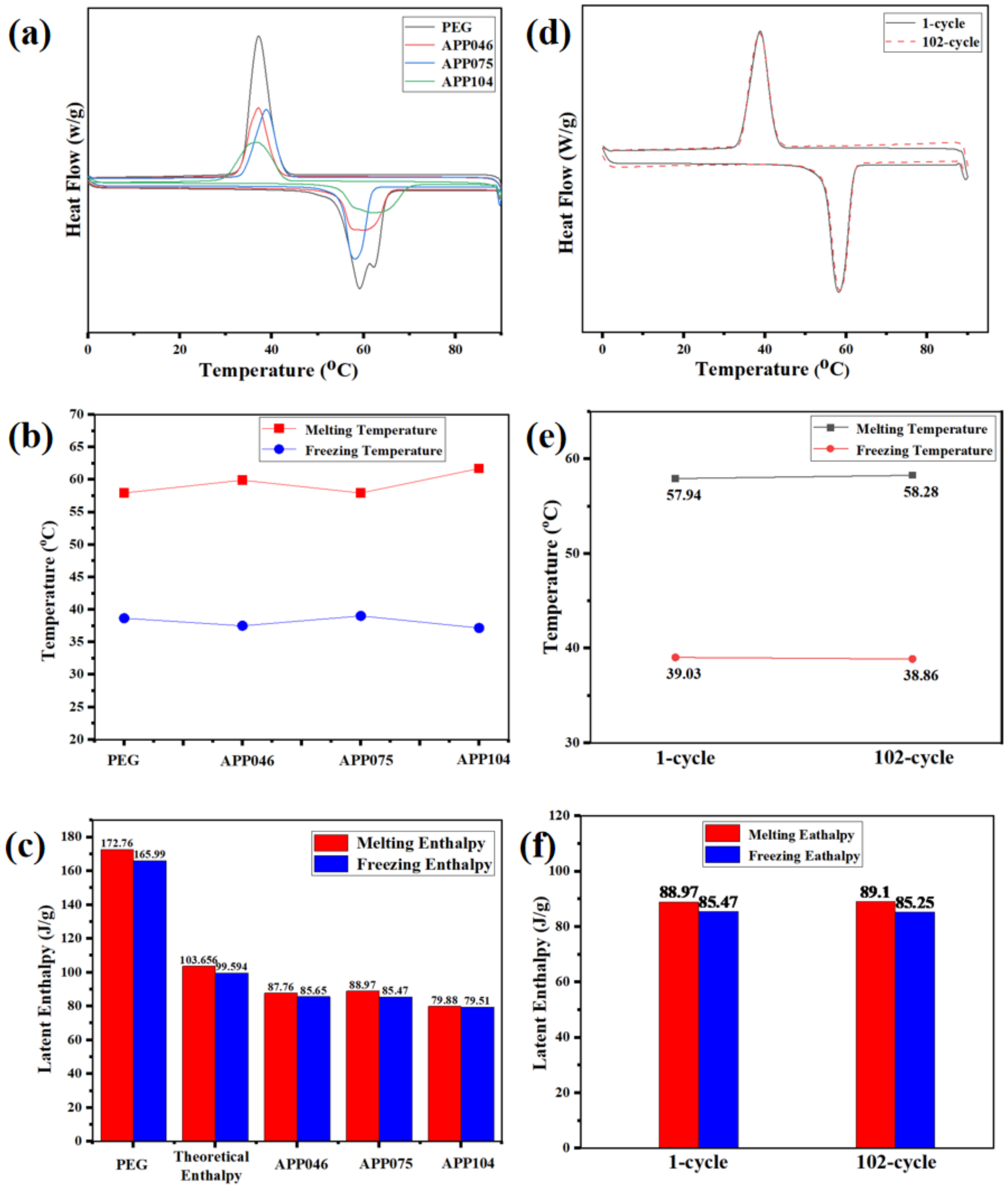

Figure 9. (a) DSC test curves and (b) phase change temperature of PEG, APP046, APP075, APP104; (c) Melting and freezing enthalpy of PEG, theoretical production, APP046, APP075, APP104; (d) DSC curves, (e) phase change temperature and (f) phase change enthalpy of APP075 before and after 102 cycles.

The thermal reliability of the APP composite fiber film plays a significant role in their long-term service for thermal energy storage. To investigate the thermal reliability of the APP composites during the working period, 102 DSC thermal cycles were performed on the APP075 composite fiber film. As shown in Figure 9 (d), the DSC curve of APP075 after 102 times thermal cycling almost overlaps with the initial DSC curve. Meanwhile, the change of phase change temperature is negligible, which is shown in Figure 9 (e). Last but not the least, as shown in Figure 9 (f), the melting and freezing enthalpies of the APP075 after 102 times thermal cycling are 88.97 J/g and 85.47 J/g, which are extremely close to those of the original APP075 (89.10 J/g and 85.25 J/g). All in all, the APP composite fiber films possess the reliability of phase change capability and have great potential for practical applications.

Table 1. Thermal characteristics of PEG and corresponding productions.

Samples	**T_m (°C)**		**ΔH_m (J/g)**	**T_c (°C)**		**ΔH_c (J/g)**
	Onset	**Peak**		**Onset**	**Peak**	
PEG	54.04	57.96	172.76	41.79	38.68	165.99
APP046	54.51	59.93	87.76	41.16	37.51	85.65
APP075	54.84	57.94	88.97	42.57	39.03	85.47
APP104	54.24	61.72	79.88	42.69	37.17	79.51

Shape stability, that is, the ability of the PCMs to maintain their shape after appropriate packaging technology (electrospinning technology), is of great significance to develop practical applications. In the leakage tests, pure PEG and APP composite fiber films were placed in an oven at a constant temperature of 80 °C, and photos of the three samples and PEG were taken to explore their exudation stability after 1 h as shown in Figure 10. Compared with pure PEG, all APPs samples prepared by electrospinning have no traces of liquid leakage on the filter papers, indicating that the migration of PEG in the APPs after melting could be effectively prevented, revealing outstanding shape stability. On the one hand, entanglement of the macromolecular chains between PVP and PEG can effectively restrict the motion of the PEG, even if the temperature was higher than the PEG melting temperature. On the other hand, the three-dimensional network structure of the polymer fibers was able to tightly confine the excess PEG. Therefore, the APP composite fiber films possess excellent shape stability and leakage resistance, which is beneficial to their application in thermal energy storage.

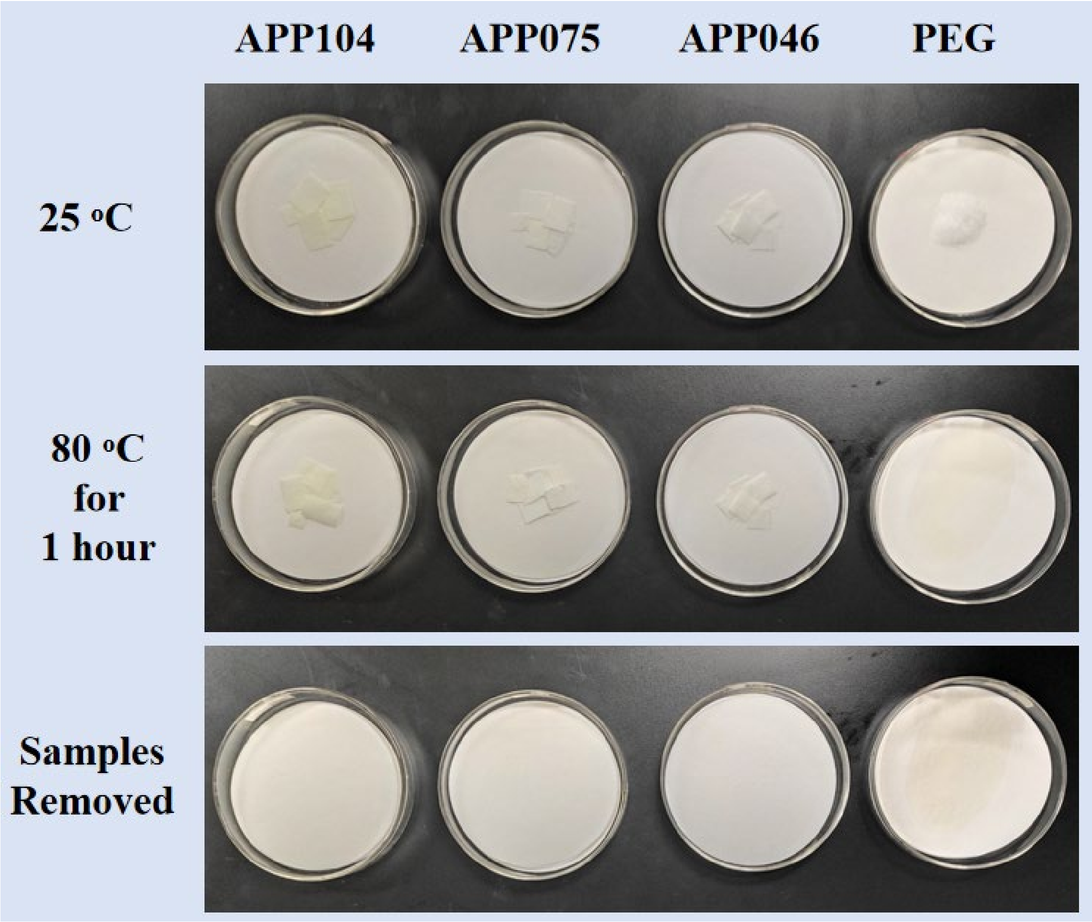

Figure 10. The digital photographs of leakage experiment of different samples and pure PEG.

3.7 Applications of the pyrene-based AIEgen/PVP/PEG (APP) composites

3.7.1 Thermal energy storage in solar-to-thermal conversion

The prepared APP composite fiber films possess a certain phase-change energy storage capacity and thermal reliability. As a result, the APP075 composite fiber film with the best energy storage effect in the samples was selected in order to study the photo-thermal conversion performance. As shown in Figure 11 (a), the APP075 composite fiber film was pressed as a cylinder with about 5mm thickness and 6 mm diameter and irradiated vertically by a simulated sunlight at different solar energy densities. The temperature was also measured using an IR camera. The corresponding images and curves are displayed in Figure 11 (b,c), and intuitively illustrate the process of thermal energy storage when the APP composites working. When the lamp is turned on to simulate sunlight, the APP075 composites under different energy densities all go through three stages. At the beginning, the temperature of the composites rose rapidly, then (160 s later), the temperature of the composites rose slowly and a thermal storage platform occurred, which is the process of solar-thermal energy storage. In this process, the temperature reached the phase change temperature, and the PEG inside of the composites starts melting to absorb solar-thermal energy, and store it in the way of latent heat. [26] Finally, with continuous sunlight illumination, the temperature continued to rise rapidly to the highest temperature. With the increase of solar energy density, the highest temperature that the APP075 composite can reach became higher. After the lamp was turned off, three stages are observed as well. At first, the temperature of the composites fell rapidly as a result of the thermal exchange to surroundings. Then, the temperature enters a plateau stage and lasts for about 200 s, which is the process of solar-thermal energy release. This is attributed to the temperature decline associated to the crystallization temperature and a liquid-solid phase change process occurred. [50] Finally, the temperature continued to rapidly decrease to room temperature. In addition, compared with the APP075 composite, the highest temperature that APP046 can reach under the same solar energy density and working time is lower, which may be caused by the lower content of **Py-CH**. The above-mentioned results demonstrate that the APP composites have promising potential for efficient solar-to-thermal energy conversion and storage.

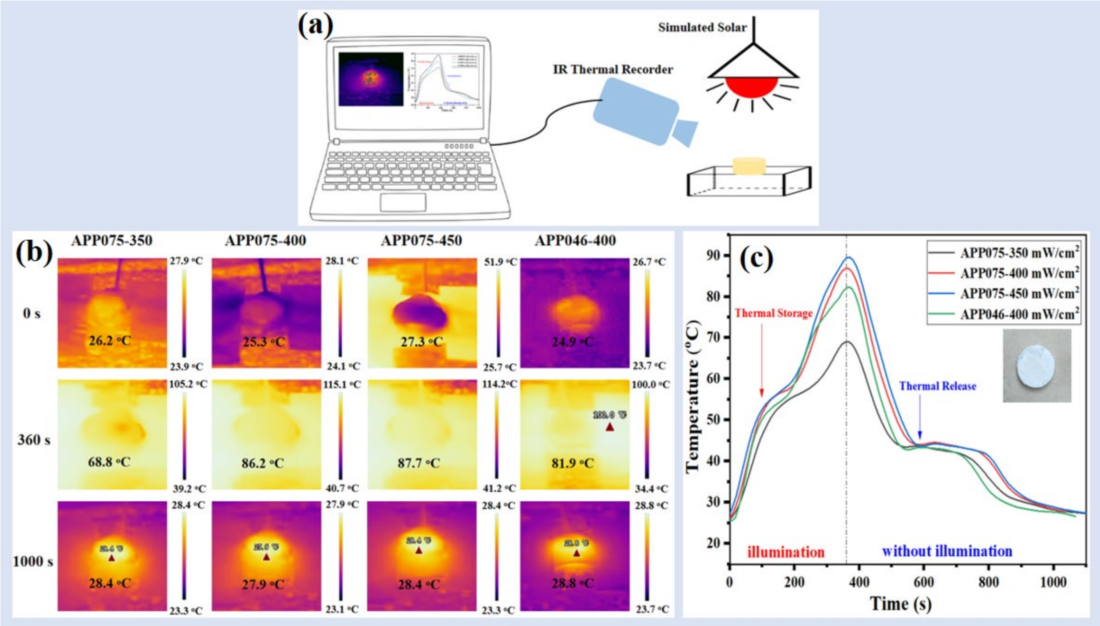

Figure 11. (a) The schematic of setup for light-thermal conversion test; (b) IR thermography pictures of APP075-350, APP075-400, APP075-450 and APP046-400; (c) time-temperature curves of APP046 and APP075 under

different power of illumination.

3.7.2 Temperature sensing and high-temperature warning

A high-temperature may not only create damage to electronic devices or even cause an explosion, but may also have an impact on human skin. Therefore, high temperature warning plays an important role in modern day life. What's more, flexible high-temperature warning materials have gained more and more attention for their wider application. [51] Due to the variable temperature fluorescence properties and fluorescent recyclability, the flexible APP composite fiber films can be extended to practical applications in flexible temperature sensing and high-temperature warning. For example, as shown in Figure 12 (a), the flexible APP075 composite fiber film was attached to the surface of the beaker filled with oil, and the beaker was placed on the heating stage to reach various temperatures. It was found that the fluorescent color of the film gradually changed with the increase of heating temperature. When the temperature reached 180 °C, the film emits light blue fluorescence under ultraviolet light, indicating that the wall of the beaker has reached a high temperature. The real application testing was carried out to prove that the flexible APP composite fiber films have an excellent temperature-warning function. Further, as shown in Figure 12 (b), under the help of the remote monitoring alarm system designed by the image recognition algorithm [52], a fluorescent color changing warning signal released by the APP composite fiber films can be gained fast even without human participation. This high-temperature warning system will be widely used in complex industrial environments (power stations, chemical plants, etc.), equipment parts of aircrafts, even for fire warning in buildings, etc.

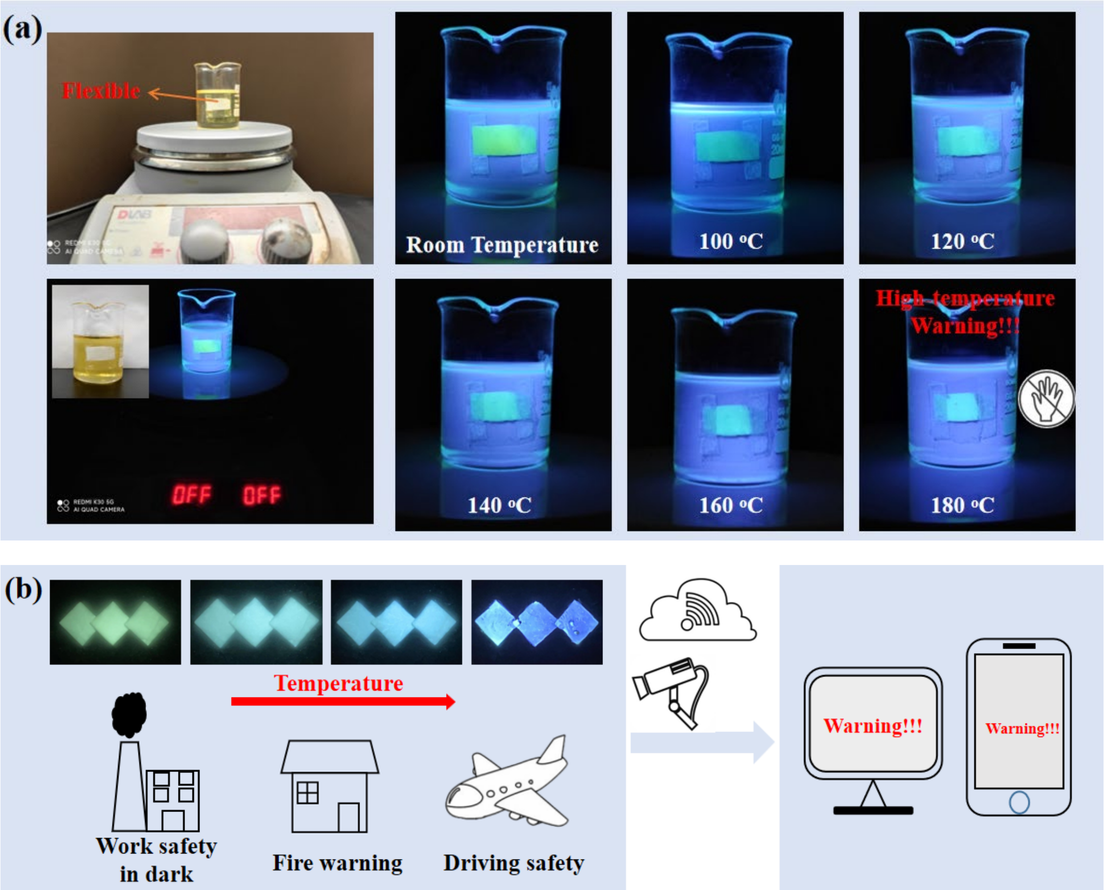

Figure 12. (a) The application of APP075 for high-temperature warning on the beaker with oil; (b) APPs can be further used for work safety, fire warning, driving safety and their combination with the remote monitoring alarm system.

3.7.3 Fluorescence anti-counterfeiting

Fluorescent dyes have been incorporated into paper money and widely used as anti-counterfeiting labels. [53] On the basis of the excellent AIE induced PL property of the prepared APP composite fiber films, luminescent images were designed by photolithography for anti-counterfeiting applications. During the experiments, it was exciting to find that fluorescent quenching occurred in the illuminated part, while the fluorescent effect was retained in the blocked part of the fiber films under irradiation of LED UV curing light. The loss of fluorescence performance can be attributed to the photocyclization of the **Py-CH** during UV irradiation, whose emission blue shifts to the invisible region. [54] Encouraged by the above mechanism, as shown in Figure 13, ‘GDUT’ with fluorescence performance and ‘GDUT’ and ‘AIE&PCM’ without fluorescence characteristic were successfully achieved. Compared with common fluorescent dyes, the fluorescent pattern can be gained with the APP composite fiber film just by the photolithography process, which decreases the complexity of the processing. Based on the obtained results, it was found that the APP composite fiber films open up a new strategy for the preparation of low-cost and simple security materials for anti-counterfeiting applications.

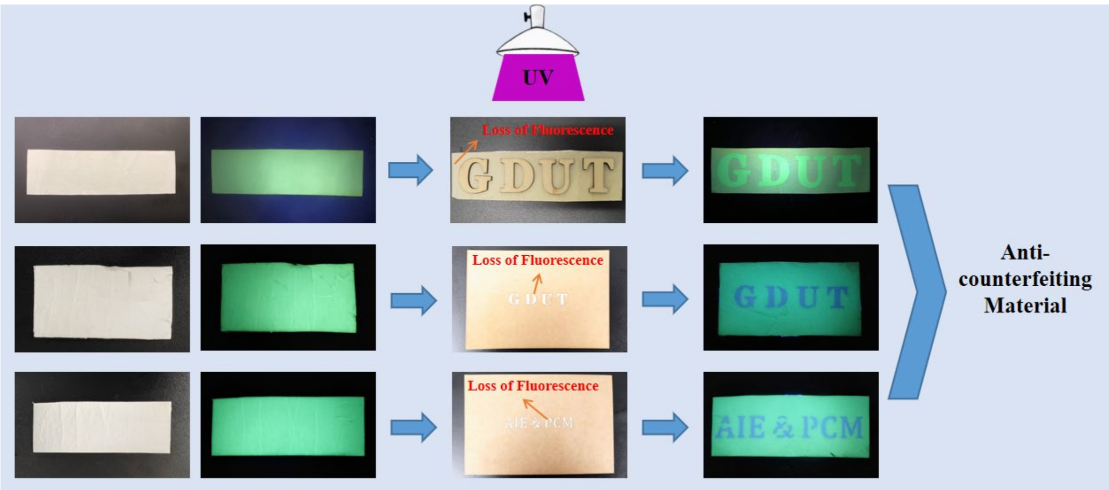

Figure 13. APPs can be used as anti-counterfeiting for their loss of fluorescence due to irradiation of UV.

4 Conclusion

In conclusion, electro spun fluorescent thermochromic APP composite fiber films were fabricated by using PEG as the PCM, PVP as the supporting matrix and water absorption material, and **Py-CH** as the fluorescent AIE material. After electrospinning, the entanglement of the macromolecular chains between PVP and PEG and the constraint force resulting from the distinctive porous structure solved the leakage problem of PEG. The APP composites not only possess thermal energy storage properties and photo-thermal conversion performance, but also have variable temperature fluorescence resulting from the combination of the AIE and TICT characteristics of **Py-CH** and the water absorption performance of the PVP. As a result, three promising applications of this novel and advanced composite were discovered, namely solar-to-thermal conversion and storage, high-temperature warning, and anti-counterfeiting.

Acknowledgments

This research was funded by the National Natural Science Foundation of China (Grant No. 52003111, 21975054 and U20A20340), National Key R&D Program of China (2020YFB0408100), the Program for Guangdong Introducing Innovative and Entrepreneurial Team (2016ZT06C412), Foshan Science and Technology Innovation Team Project (1920001000108). CR thanks the University of Hull for support.

References

1. Bai H, Li C, Shi G (2011) Functional composite materials based on chemically converted graphene. Advanced Materials 23:1089-1115. https://doi.org/10.1002/adma.201003753
2. Hamidi F, Aslani F (2019) Additive manufacturing of cementitious composites: Materials, methods, potentials, and challenges. Construction and Building Materials 218:582-609. https://doi.org/10.1016/j.conbuildmat.2019.05.140
3. Hsissou R, Seghiri R, Benzekri Z, et al (2021) Polymer composite materials: A comprehensive review. Composite structures 262:113640. https://doi.org/10.1016/j.compstruct.2021.113640
4. Cao Y, Weng M, Mahmoud M, et al (2022) Flame-retardant and leakage-proof phase change composites based on MXene/polyimide aerogels toward solar thermal energy harvesting. Advanced Composites and Hybrid Materials 5:1253-1267. https://doi.org/10.1007/s42114-022-00504-4
5. Rajak DK, Pagar DD, Kumar R, et al (2019) Recent progress of reinforcement materials: a comprehensive overview of composite materials. Journal of Materials Research and Technology 8:6354-6374. https://doi.org/10.1016/j.jmrt.2019.09.068
6. Cao Y, Zeng Z, Huang D, et al (2022) Multifunctional phase change composites based on biomass/MXene-derived hybrid scaffolds for excellent electromagnetic interference shielding and superior solar/electro-thermal energy storage. Nano Research 15:8524-8535. https://doi.org/10.1007/s12274-022-4626-6
7. Alva G, Lin Y, Fang G (2018) An overview of thermal energy storage systems. Energy 144:341-378. https://doi.org/10.1016/j.energy.2017.12.037
8. Da Cunha JP, Eames P (2016) Thermal energy storage for low and medium temperature applications using phase change materials–a review. Applied energy 177:227-238. https://doi.org/10.1016/j.apenergy.2016.05.097
9. Shen R, Weng M, Zhang L, et al (2022) Biomass-based carbon aerogel/Fe3O4@ PEG phase change composites with satisfactory electromagnetic interference shielding and multi-source driven thermal management in thermal energy storage. Composites Part A: Applied Science and Manufacturing 163:107248. https://doi.org/10.1016/j.compositesa.2022.107248
10. Yuan K, Shi J, Aftab W, et al (2020) Engineering the thermal conductivity of functional phase-change materials for heat energy conversion, storage, and utilization. Advanced Functional Materials 30:1904228. https://doi.org/10.1002/adfm.201904228
11. Wei D, Weng M, Mahmoud M, et al (2022) Development of novel biomass hybrid aerogel supported composite phase change materials with improved light-thermal conversion and thermal energy storage capacity. Advanced Composites and Hybrid Materials 5:1910-1921. https://doi.org/10.1007/s42114-022-00519-x

12. Huang X, Alva G, Jia Y, et al (2017) Morphological characterization and applications of phase change materials in thermal energy storage: A review. Renewable and Sustainable Energy Reviews 72:128-145. https://doi.org/10.1016/j.rser.2017.01.048
13. Zhu C, Lu X, Wu H, et al (2022) Constructing heat conduction path and flexible support skeleton for PEG-based phase change composites through salt template method. Composites Science and Technology 226:109532. https://doi.org/10.1016/j.compscitech.2022.109532
14. Mohamed NH, Soliman FS, El Maghraby H, et al (2017) Thermal conductivity enhancement of treated petroleum waxes, as phase change material, by α nano alumina: Energy storage. Renewable and Sustainable Energy Reviews 70:1052-1058. https://doi.org/10.1016/j.rser.2016.12.009
15. Liu Y, Yang H, Wang Y, et al (2021) Fluorescent thermochromic wood-based composite phase change materials based on aggregation-induced emission carbon dots for visual solar-thermal energy conversion and storage. Chemical Engineering Journal 424:130426. https://doi.org/10.1016/j.cej.2021.130426
16. Chen C, Wang L, Huang Y (2007) Electrospinning of thermo-regulating ultrafine fibers based on polyethylene glycol/cellulose acetate composite. Polymer 48:5202-5207. https://doi.org/10.1016/j.polymer.2007.06.069
17. Meng Y, Zhao Y, Zhang Y, et al (2020) Induced dipole force driven PEG/PPEGMA form-stable phase change energy storage materials with high latent heat. Chemical Engineering Journal 390:124618. https://doi.org/10.1016/j.cej.2020.124618
18. Wang C, Wang L, Liang W, et al (2022) Enhanced light-to-thermal conversion performance of all-carbon aerogels based form-stable phase change material composites. Journal of Colloid and Interface Science 605:60-70. https://doi.org/10.1016/j.jcis.2021.07.066
19. Sundararajan S, Samui AB, Kulkarni PS (2017) Versatility of polyethylene glycol (PEG) in designing solid–solid phase change materials (PCMs) for thermal management and their application to innovative technologies. Journal of Materials Chemistry A 5:18379-18396. https://doi.org/10.1039/C7TA04968D
20. Karaman S, Karaipekli A, Sarı A, et al (2011) Polyethylene glycol (PEG)/diatomite composite as a novel form-stable phase change material for thermal energy storage. Solar Energy Materials and Solar Cells 95:1647-1653. https://doi.org/10.1016/j.solmat.2011.01.022
21. Babapoor A, Karimi G, Golestaneh SI, et al (2017) Coaxial electro-spun PEG/PA6 composite fibers: fabrication and characterization. Applied Thermal Engineering 118:398-407. https://doi.org/10.1016/j.applthermaleng.2017.02.119
22. Wu B, Lao D, Fu R, et al (2020) Novel PEG/EP form-stable phase change materials with high thermal conductivity enhanced by 3D ceramics network. Ceramics International 46:25285-25292. https://doi.org/10.1016/j.ceramint.2020.06.321
23. Xu C, Zhang H, Fang G (2022) Review on thermal conductivity improvement of phase change materials with enhanced additives for thermal energy storage. Journal of Energy Storage 51:104568. https://doi.org/10.1016/j.est.2022.104568
24. Ji R, Zhang Q, Zhou F, et al (2021) Electrospinning fabricated novel poly (ethylene glycol)/graphene oxide composite phase-change nano-fibers with good shape stability for thermal regulation. Journal of Energy Storage 40:102687. https://doi.org/10.1016/j.est.2021.102687

25. Luo Y, Xie Y, Jiang H, et al (2021) Flame-retardant and form-stable phase change composites based on MXene with high thermostability and thermal conductivity for thermal energy storage. Chemical Engineering Journal 420:130466. https://doi.org/10.1016/j.cej.2021.130466
26. Huang J, Su J, Xu W, et al (2022) High enthalpy efficiency lignin-polyimide porous hybrid aerogel composite phase change material with flame retardancy for superior solar-to-thermal energy conversion and storage. Solar Energy Materials and Solar Cells 248:112036. https://doi.org/10.1016/j.solmat.2022.112036
27. Xia Q, Zhang Y, Li Y, et al (2022) A historical review of aggregation-induced emission from 2001 to 2020: A bibliometric analysis. Aggregate 3:e152. https://doi.org/10.1002/agt2.152
28. Islam MM, Hu Z, Wang Q, et al (2019) Pyrene-based aggregation-induced emission luminogens and their applications. Materials Chemistry Frontiers 3:762-781. https://doi.org/10.1039/C9QM00090A
29. Yang Y, Liu S, Zhang G, et al (2023) Cellulose nanofiber encapsulated polyethylene glycol phase change composites containing AIE-gen for monitoring leak process. Composites Part A: Applied Science and Manufacturing:107452. https://doi.org/10.1016/j.compositesa.2023.107452
30. Figueira-Duarte TM, Mullen K (2011) Pyrene-based materials for organic electronics. Chemical reviews 111:7260-7314. https://doi.org/10.1021/cr100428a
31. Feng X, Hu JY, Redshaw C, et al (2016) Functionalization of pyrene to prepare luminescent materials—typical examples of synthetic methodology. Chemistry–A European Journal 22:11898-11916. https://doi.org/10.1002/chem.201600465
32. Trattnig R, Pevzner L, Jäger M, et al (2013) Bright Blue Solution Processed Triple-Layer Polymer Light-Emitting Diodes Realized by Thermal Layer Stabilization and Orthogonal Solvents. Advanced Functional Materials 23:4897-4905. https://doi.org/10.1002/adfm.201300360
33. Ni X-l, Zeng X, Redshaw C, et al (2011) Ratiometric fluorescent receptors for both Zn2+ and H2PO4–ions based on a pyrenyl-linked triazole-modified homooxacalix [3] arene: A potential molecular traffic signal with an RS latch logic circuit. The Journal of Organic Chemistry 76:5696-5702. https://doi.org/10.1021/jo2007303
34. Wang X, Wang L, Mao X, et al (2021) Pyrene-based aggregation-induced emission luminogens (AIEgens) with less colour migration for anti-counterfeiting applications. Journal of Materials Chemistry C 9:12828-12838. https://doi.org/10.1039/D1TC03022A
35. Teo WE, Ramakrishna S (2006) A review on electrospinning design and nanofibre assemblies. Nanotechnology 17:R89. https://doi.org/10.1088/0957-4484/17/14/R01
36. Zdraveva E, Fang J, Mijovic B, et al (2015) Electrospun Poly(vinyl alcohol)/Phase Change Material Fibers: Morphology, Heat Properties, and Stability. Industrial & Engineering Chemistry Research 54:8706-8712. https://doi.org/10.1021/acs.iecr.5b01822
37. Niu L, Li X, Zhang Y, et al (2022) Electrospun Lignin-Based Phase-Change Nanofiber Films for Solar Energy Storage. ACS Sustainable Chemistry & Engineering 10:13081-13090. https://doi.org/10.1021/acssuschemeng.2c03462
38. Crawford AG, Liu Z, Mkhalid IA, et al (2012) Synthesis of 2-and 2, 7-Functionalized Pyrene Derivatives: An Application of Selective C□ H Borylation. Chemistry–A European Journal 18:5022-5035. https://doi.org/10.1002/chem.201103774

39. Sreenivasulu C, Satyanarayana G (2018) Zinc-Chloride-Promoted Domino Reaction of Phenols with Terminal Alkynes under Solvent-Free Conditions: An Efficient Synthesis of Chromenes. European Journal of Organic Chemistry 2018:2846-2857. https://doi.org/10.1002/ejoc.201800391
40. Crawford AG, Dwyer AD, Liu Z, et al (2011) Experimental and theoretical studies of the photophysical properties of 2-and 2, 7-functionalized pyrene derivatives. Journal of the American Chemical Society 133:13349-13362. https://doi.org/10.1021/ja2006862
41. McRae EG, Kasha M (1958) Enhancement of phosphorescence ability upon aggregation of dye molecules. The Journal of Chemical Physics 28:721-722. https://doi.org/10.1063/1.1744225
42. Sasaki S, Suzuki S, Sameera W, et al (2016) Highly twisted N, N-dialkylamines as a design strategy to tune simple aromatic hydrocarbons as steric environment-sensitive fluorophores. Journal of the American Chemical Society 138:8194-8206. https://doi.org/10.1021/jacs.6b03749
43. Sasaki S, Suzuki S, Igawa K, et al (2017) The K-region in pyrenes as a key position to activate aggregation-induced emission: effects of introducing highly twisted n, n-dimethylamines. The Journal of Organic Chemistry 82:6865-6873. https://doi.org/10.1021/acs.joc.7b00996
44. Kéri O, Bárdos P, Boyadjiev S, et al (2019) Thermal properties of electrospun polyvinylpyrrolidone/titanium tetraisopropoxide composite nanofibers. Journal of Thermal Analysis and Calorimetry 137:1249-1254. https://doi.org/10.1007/s10973-019-08030-0
45. MacKenzie, A.P., Rasmussen, D.H (1972) Interactions in the Water-Polyvinylpyrrolidone System at Low Temperatures. In: Jellinek, H.H.G. (eds) Water Structure at the Water-Polymer Interface. Springer. https://doi.org/10.1007/978-1-4615-8681-4_12
46. Borrmann D, Danzer A, Sadowski G (2022) Water Sorption in Glassy Polyvinylpyrrolidone-Based Polymers. Membranes 12:434. https://doi.org/10.3390/membranes12040434
47. Zhang J, Zhang H, Lam JW, et al (2021) Restriction of intramolecular motion (RIM): investigating AIE mechanism from experimental and theoretical studies. Chemical Research in Chinese Universities 37:1-15. https://doi.org/10.1007/s40242-021-0381-6
48. Wang P, Zhang W, Wang L, et al (2021) Synthesis of Superabsorbent Polymer Hydrogels with Rapid Swelling: Effect of Reaction Medium Dosage and Polyvinylpyrrolidone on Water Absorption Rate. Langmuir 37:14614-14621. https://doi.org/10.1021/acs.langmuir.1c02295
49. Zhang W, Wang P, Deng Y, et al (2021) Preparation of superabsorbent polymer gel based on PVPP and its application in water-holding in sandy soil. Journal of Environmental Chemical Engineering 9:106760. https://doi.org/10.1016/j.jece.2021.106760
50. Li W, Zhai D, Gu Y, et al (2022) 3D zirconium phosphate/polyvinyl alcohol composite aerogels for form-stable phase change materials with brilliant thermal energy storage capability. Solar Energy Materials and Solar Cells 239:111681. https://doi.org/10.1016/j.solmat.2022.111681
51. Wang J, He J, Ma L, et al (2020) Multifunctional conductive cellulose fabric with flexibility, superamphiphobicity and flame-retardancy for all-weather wearable smart electronic textiles and high-temperature warning device. Chemical Engineering Journal 390:124508. https://doi.org/10.1016/j.cej.2020.124508
52. Fu T, Zhao X, Chen L, et al (2019) Bioinspired color changing molecular sensor toward early fire detection based on transformation of phthalonitrile to phthalocyanine. Advanced Functional Materials 29:1806586. https://doi.org/10.1002/adfm.201806586

53. Qi Q, Liu Y, Fang X, et al (2013) AIE (AIEE) and mechanofluorochromic performances of TPE-methoxylates: Effects of single molecular conformations. RSC Adv 3:7996-8002. https://doi.org/10.1039/C3RA40734A

54. Liu S, Cheng Y, Li Y, et al (2020) Manipulating solid-state intramolecular motion toward controlled fluorescence patterns. ACS nano 14:2090-2098. https://doi.org/10.1021/acsnano.9b08761